AD-A146 761 THEORETICAL AND EXPERIMENTAL MODAL ANALYSIS OF A ROTOR 1/1
TEST RIG(U) ADMIRALTY MARINE TECHNOLOGY ESTABLISHMENT
TEDDINGTON (ENGLAND) D A CORDNER AUG 83
UNCLASSIFIED AMTE(N)/TM83079 DRIC-BR-92591 F/G 20/1 NL

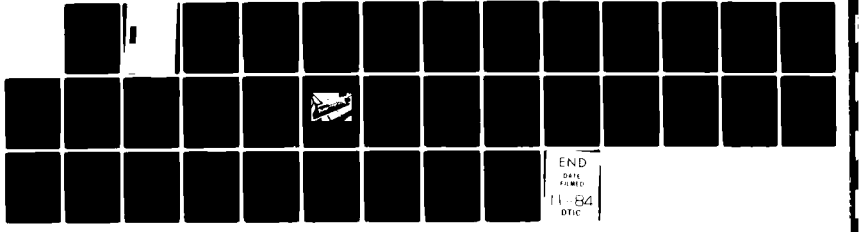

END
DATE FILMED
11-84
DTIC

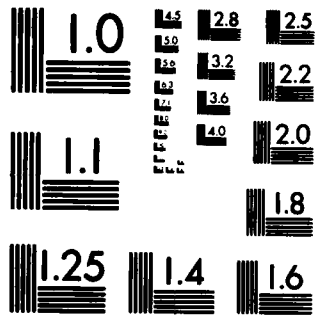

MICROCOPY RESOLUTION TEST CHART
NATIONAL BUREAU OF STANDARDS-1963-A

AMTE(N)TM83079

THEORETICAL AND EXPERIMENTAL MODAL ANALYSIS OF A ROTOR TEST RIG (U)

By

D A Cordner

Summary

As part of a programme for understanding the vibration of shipboard machinery a modal analysis was performed on an experimental rig consisting of a rotor/motor assembly connected to a base plate mounted on a test bed. Two methods were used; firstly a modal software package for the calculation of modal parameters from experimental data and secondly a theoretical model using the coupling of dynamic stiffness matrices. A comparison of the results is made. (U).

AMTE(Teddington)
Queens Road
TEDDINGTON Middx TW11 OLN

August 1983

Pages 40
Figures 18

CONTENTS

INTRODUCTION

Noise and vibration of large machinery complexes is a major problem on ships. As part of a larger programme for understanding and chacterising the vibration of shipboard machinery in order to reduce the noise levels, various machinery items are modelled experimentally and theoretically. The aim of this memorandum is to look at the merits of two modelling systems applied to a rotor test rig; and to determine the areas in which each method would be suitable for modelling larger machinery structures. One of the methods is purely theoretical, the other is experimental but based on established modal analysis theory.

A dynamic analysis was carried out on an experimental rig consisting of a rotor/motor assembly connected to a base plate mounted on a test bed. This rig had originally been designed to study the transmission of vibration using various types of ball bearings. For the purposes of this memorandum it is merely an experimental rig which provided a convenient system on which to perform a modal analysis by theoretical and experimental methods. The analysis was static: at no time was the motor running.

The experimental method involved the use of a General Radio computer with a PDP 11/34 processor (hereafter referred to as the Genrad), and a Genrad SDRC modal software package for the collection and analysis of experimental modal data. The theoretical analysis was carried out using a computer program for the mathematical modelling of structures through substructuring and the addition of dynamic stiffness matrices for the substructures.

A photograph of the test rig is given in Figure 1(a) and a diagram labelling the separate parts of the rig in Figure 1(b). It is seen that the rig consists of a motor attached via a drive rod to a rotor. This is attached to the base plate at three positions; at the motor, at the rotor, and about one third of the distance along from the motor end by the clutch and brake units. The base plate is seated on eight X-mounts - four along each of the longer sides of the base plate - which are attached to the test bed. The directions of motion investigated were the Y, vertical direction, for the rotor and the base plate, and the Z, transverse horizontal direction, for the rotor on the base plate.

The details of the experimental measurements are given in Section 2, together with an outline of the theory behind the analysis. The rig was excited by impact testing and measurements were taken of the acceleration and force at selected points in order to provide inertance plots and mode shapes.

Details of the mathematical modelling are given in Section 3. The structure was analysed in essentially two parts; the flexural vibrations of the rotor were analysed by modelling it as a series of beams and the base plate was analysed for out of plane vibrations. These two components were then coupled to produce a dynamic stiffness matrix for the composite structure. The horizontal flexure of the motor was modelled by introducing beams for the supports between rotor and plate and fixing the lower ends to ground to model the absence of horizontal plate motion. By introducing the supporting beams into the out of plane model it was possible to evaluate their effects on the vibration of the structure.

A discussion of the results is given in Section 4, together with a comparison of the two sets of data indicating the areas of agreement and disagreement between the results of the two methods.

2. EXPERIMENTAL MEASUREMENTS ON THE ROTOR TEST RIG

2.1 Details of the Measurement Technique

A set of measurement locations was defined on the base plate. A plan view of the plate, together with measurement locations, is given in Figure 2. All measurements on the plate were made perpendicular to the plane of the plate. The plate dimensions are 1.42m x 0.33m x 0.030m thick. A line diagram of the instrumentation used in the experiment is given in Figure 3. A B and K type 4333 accelerometer was placed at position 28 on Figure 2 and the measured response was taken to the Genrad via a B and K charge amplifier calibrated to give a 1 volt output for a $1ms^{-2}$ acceleration. An impact force was applied using an instrumental hammer and the force response was taken to the Genrad via a B and K charge amplifier calibrated to give a 1 volt output for a 1 newton force. The accelerometer remained mounted at position 28 throughout the testing of the base plate and the hammer was moved around the test positions. By reciprocity the results obtained are equivalent to those that would be obtained by striking at one position on the plate and having a set of accelerometers at other locations. The use of reciprocity assumes the linear behaviour of the structure. Some measurements were made to check reciprocity, with reasonable results.

A set of forcing positions was marked along the top of the rotor to evaluate the mode shapes for the motion in the same direction as the out of plane vibrations of the plate, and along the side of the rotor to calculate the mode shapes for the side to side vibration of the rotor. The same reference location (ie location 28 on the base plate) was used so that the correct phase relationships could be obtained to produce mode shapes for the plate and rotor combined. The measurement locations are given in Figure 4.

2.2 Details of the Modal Analysis Technique

The Genrad SDRC modal software package is designed to analyse experimental modal data for resonant frequencies, modal damping and mode shapes. Two input channels were used for force and acceleration respectively. Dividing the acceleration by the force gives the inertance response under the assumption that the test rig is a linear system. (The data was stored on disc using the program DATM(1) which provides a set of routines for the collection of experimental data). For each forcing location ten separate impacts were made and the results averaged to give the inertance plots. When all the experimental data had been obtained, analysis was performed using the set of programs contained in MODAL (2). From each plot it is possible to select visually a number of frequencies corresponding to peaks, where the resonances are thought likely to be located. (It is important to realise that a peak on the transfer function does not necessarily indicate that a resonance is located at that frequency, particularly under conditions of high modal overlap; instead a peak corresponds to the inphase response of all nearby modes (3). However, for the first few modes it is reasonable to expect that the number of peaks corresponds to the number of modes provided that measurement is away from the

nodal points and the resolution is sufficient). The software then calculates a set of modal parameters associated with these selected frequencies and a corresponding inertance plot is produced. This plot is displayed on the screen together with the original experimental plot and the user is invited to accept or reject the fit. If the fit is accepted then estimates are provided of the resonant frequency and viscous damping ratio associated with each mode. These two parameters are estimates only and are obtained by implementing least square fits to Nyquist circles for resonant modes using single degree of freedom models. The method is applicable to both simple isolated modes and to the case of higher modal overlap where the Nyquist circles are distorted by the presence of adjacent modes. It sometimes happens that no mode can be produced from a peak identified on the screen in which case the program will state that there is no mode near that frequency. This does not mean that there is no mode present - merely that the software is unable to locate one. This sometimes happens when a mode is at a low level or appears heavily damped. All the main resonances are identified. The estimated resonant frequency produced by the software is determined by comparison of the inphase and out of phase components around the visually selected frequency. The estimated and selected resonant frequencies are not necessarily identical but will normally lie close to each other.

Having estimated the resonant frequencies and damping it is possible to generate mode shapes for the entire structure. The geometry of the structure is defined within the program by the user specifying the coordinates of the measurement locations. In order to define the structure adequately there must be sufficient measurement locations for there to be no more than one half wavelength between adjacent positions; otherwise a problem can occur similar to aliasing in digital signal processing. Using the estimated value of the resonance frequency and modal damping for the first mode, single degree of freedom fits are applied to the Nyquist circle of each transfer function. At this stage the user has the opportunity to inspect each fit and to accept or reject it or alter the frequency range of the data used in order to improve the fit. Having calculated the modal amplitude and phase at each position a mode shape is produced. This mode shape may be viewed either statically or dynamically from a variety of projections. This process is repeated for all subsequent modes. It is not normally possible to obtain all the resonances from one inertance plot because the forcing or response location may be close to a structural node. The point inertance is a good measurement to take for the first estimate and this will mean that no more than one nodal position can be involved. However, checks were made with other plots, to ensure that no resonances had been missed, and with the point inertance obtained elsewhere to ensure that the transducers were moved away from the potential nodal point.

A major limitation on the method is the assumption of uniform damping throughout the structure. It is often the case in practice that the damping is localized to certain regions of the structure, especially at the junctions between different parts of a structure (4). Another problem with damping is the difficulty in obtaining consistent sets of results. If the modal parameters are obtained from the same inertance plot it is found that, although the resonant frequencies are virtually unchanged, the estimates of damping may

vary by over 50%. This arises because the resonant peaks are not sharp; consequently a slightly different set of points is taken from the plot to define the resonant peaks and this means that the modal frequencies are slightly different giving rise to errors in damping. By estimating modal parameters at different positions across the structure there is a small variation in resonant frequencies and a very large variation in damping. Although the model assumes a constant damping throughout the structure for each individual mode, as a real structure the test rig exhibits variation in damping. It was originally hoped that some indication of this variation in damping across the structure could be obtained by measuring the driving point inertance at different points on the structure, but the large uncertainty associated with values of damping prevents this.

2.3 Production of the Modal Data for the Rotor Test Rig

As may be seen from Figure 2 there are thirty-two measurement locations marked on the base plate. The driving point inertance obtained at position 28 is given in Figure 5(a). A number of peaks may be identified in Figure 5(a) and these were entered as first visual estimates of resonant frequencies using a cursor on the screen to pinpoint the peaks. These values were then used in the software package to produce a set of modal parameters and a response curve from these parameters. This was repeated a few time on the same inertance plot and a small variation (about 2%) was obtained in the frequencies of the modes and a large variation in damping. It is somewhat disconcerting that there is this variation in parameter values.

The estimated modal parameters at the driving point for the first eight modes are given below. The quoted values are sample values taken from one set of peaks selected from a single inertance measurement, and are not meant to be taken as average values. The only averaging occurs when the results of ten impacts are averaged to give one inertance plot. The mode shapes were generated over the plate by performing a single degree of freedom fit for each mode over all positions. The mode shapes are designated (i, j), in which the first number refers to the number of half-wavelengths in the mode shape along the longer sides of the plate and the second number along the shorter sides. Plate modes are either symmetric or antisymmetric about the mid-points of the sides. (It should be noted that the notation (i, j) refers to the number of half-wavelengths in the corresponding mode of a plate with fixed sides and is used for a completely free plate by convention).

Mode Number	Frequency	Damping	Mode Designation
(-	46.8	0.276	(3,1) doubly symmetric)
1	66.2	0.0285	(3,1) doubly symmetric
2	110.8	0.0359	
3	132.8	0.0257	(2,2) doubly antisymmetric
4	155.6	0.0108	(4,1) antisymmetric-symmetric
5	178.6	0.0343	(3,2) symmetric-antisymmetric
6	231.6	0.00901	(5,1) doubly symmetric
7	304.5	0.0241	
8	426.3	0.0108	

For a completely free plate the first three modes, (1,1), (2,1) and (1,2) are a translational and two rotational rigid body modes.

The bracketed mode is suspect because of the high level of damping associated with it. By comparing these results with other inertance plots, see for example Figure 5(b-d), at other positions, it was found that all the major resonances had been identified up to the eighth mode.

Both the bracketed mode and the first mode, despite their frequency separation, produced mode shapes corresponding to the first (3,1) doubly symmetric mode. It is not physically possible for any mode shape to have two distinct frequencies in a linear system. Hence the mode shapes must be slightly different at 47Hz and 66Hz, but the experimental procedure did not use a fine enough grid to produce the differences in mode shape. The third mode at 132.8Hz is the first doubly antisymmetric (2,2) plate mode. The fourth mode at 155.6Hz is an antisymmetric-symmetric (4,1) plate mode. The fifth mode is a symmetric-antisymmetric (3,2) mode. The sixth mode is a doubly symmetric (5,1) mode. Some of these modes on the plate are shown in Figure 6. The hard line indicates the deformed shape and the dotted line the undeformed shape. The second mode at about 110Hz is seen from Figure 5 to be at a low level compared with other modes; there is no reasonable mode shape seen on the plate for this mode and, as is shown later, this mode is mainly associated with the rotor.

Measurements were then made on the rotor in two directions: firstly in the same direction as on the plate to produce the vertical flexural vibrations, and then in a horizontal plane to produce horizontal flexural vibrations. No forcing was done along the line of the axis of the rotor and no attempt was made to excite torsional modes. The impact force was applied at positions 35Y to 42Y indicated in Figure 4 along the top of the rotor. The corresponsing positions for horizontal forcing were the same positions turned through an angle of 90°, except at the far end, position 42, where no measurement was taken horizontally due to the inaccessibility of the rotor in the housing.

For modes appearing on the rotor it is essential to be able to distinguish between the antisymmetric and the symmetric plate modes. If the axis of the rotor occurs along a nodal line the vibration in the plate will not be transmitted or will only be weakly transmitted to the rotor. This is because the supports on which the rotor is seated are symmetrical about this nodal line and extend only a small distance from this line compared with the plate length, and there is thus no path by which much energy can flow to the rotor. The rotor will lie along a nodal line if the plate mode shape is antisymmetrical along the shorter sides. It does not matter, for the purpose of determining the nodal line of the rotor, whether the mode is symmetrical or antisymmetrical along the longer sides.

The first doubly symmetric (3,1) plate mode appears as a flexural mode in a vertical plane through the rotor axis. The doubly antisymmetric (2,2) plate mode does not appear on the rotor. This is as expected for antisymmetric modes. The next mode at 155.6Hz is an antisymmetric-symmetric plate mode in which the nodal lines are between the mid-points of the longer sides and the line of the rotor does not appear as a nodal line. Hence the plate mode does appear on the rotor as vertical vibration. The next plate mode at 178Hz does not appear on the rotor because it falls along a nodal line.

The horizontal motion of the rotor was measured by placing the accelerometer at position 39Z - (positive and negative directions are shown in figure 4) and then measuring the response when the impact was acting either horizontally or vertically on the rotor. The change in accelerometer position was made so that the response could be measured horizontally on the rotor. Since measurements had already been obtained from forcing on the rotor with the accelerometer on the base plate, phase relationships had already been constructed for the complete system. The modes together with the damping associated with them (found from inertance measurements at positions 38Z-, 39Z- and 40Z-) are given below.

Mode	Frequency	Damping
1	103.6	0.127
2	149.1	0.0797
3	205.4	0.0106
4	257.7	0.0236
5	479.0	0.0222

The driving point inertance at position 39Z-, and some other measurements on the rotor, are given in Figure 7. Some mode shapes are given for the horizontal flexure of the rotor in Figure 8. Up as far as the third mode all the modes appear to have similar shapes. This mode shape is confined almost entirely to the end of the rotor away from the motor between the clutch and brake support and the end. The 205Hz mode appears along the length of the rotor, with a nodal point by the clutch and brake support. The 103.6Hz mode corresponds with the 110Hz mode seen on the plate, at a low level. Generally very little vibration occurs on the plate due to horizontal flexure of the rotor because the motion is at right-angles to out-of-plane plate vibration.

3. MATHEMATICAL MODELLING OF THE ROTOR TEST RIG

3.1 Description of the Modelling Technique

The program used was a dynamic stiffness coupling technique for the building up of structures from the coupling of dynamic stiffness matrices of component substructures. The program was written in FORTRAN by Sainsbury (5) and has been extended at AMTE and implemented on a PDP 11/34 minicomputer. A set of coordinates representing the degrees of freedom are defined on the structure, which is subsequently divided into substructures. The division is performed in such a way as to produce simple substructures whose dynamic stiffness matrices can easily be found. The dynamic stiffness matrix can be built up for each substructure by defining a set of forces or moments that can be applied to the substructure, and a set of responses. When a dynamic stiffness matrix has been produced for each substructure these matrices are added to produce a system dynamic stiffness matrix. The solutions are exact in so far as the parameters for the subsystems can be accurately specified, with the limitation that the assumption of point connections between components is approximate. The subroutines for calculating the dynamic stiffness

matrices of mass-spring systems and beams agree exactly with theory. The theory for the dynamic stiffness of beams is based on (6), (7). It is also possible to enter theoretical or experimental data from other sources to produce the dynamic stiffness matrices of substructures. It is possible to calculate inertance, mobility or receptance, in the form of real and imaginary parts, or amplitude and phase, for a number of forcing and response locations.

3.2 Application of the Modelling Technique to the Rotor Test Rig

The modelling was carried out similarly to the experimental analysis: the dynamic stiffness matrix was found for the rotor on its own, and for the base plate on its own, and these matrices were added to give a system dynamic stiffness matrix. The coupling occurred at three points, representing the three supports between plate and rotor, and at each of these points the model had three degrees of freedom representing the out of plane degrees of freedom of the plate. Since the coupling was modelled as occurring at three points connecting the plate and rotor the model was too stiff, since, unlike the real structure, there was no separation of the planes of the rotor and plate and the system behaved as a beam stiffened plate. The whole system was modelled as freely suspended since it was believed that the X-mounts (having a very low resonant frequency) by which the plate was fixed to the test bed, would not significantly affect the vibration characteristics of the structure except by introducing damping. The eigenfrequencies of the plate were found by dividing it up into finite elements using thin plate theory with rectangular elements containing a set of four non-conforming nodes at the corners (8). The reason for using a finite element model rather than tables of eigenfrequencies was to obtain the response at a set of frequencies at regular intervals across the plate regardless of whether these frequencies coincided with eigenfrequencies. From a forced response the dynamic stiffness matrix was found for the plate. The division of the plate into elements with element numbers and node numbers is given in Figure 9; there are three degrees of freedom at each node. The two elements at the motor end were 0.1016m long by 0.165m wide; all the other elements were 0.1473m long by 0.165m wide. The thickness of the elements was 0.030m, the thickness of the base plate. The first few eigenfrequencies produced by the finite element analysis were at 77Hz, 203Hz, 217Hz, 420Hz and 430Hz. The accuracy of the analysis was found to be very good and agreement was obtained with theoretical exact values for the eigenfrequencies of a completely free rectangular plate (9).

The rotor was modelled as a series of Timoshenko beams in flexure which include the effects of shear and rotary inertia. A dynamic stiffness matrix was formed by considering the vertical vibrations of the rotor with three degrees of freedom at each end of the beam, producing a 6 x 6 subsystem dynamic stiffness matrix for each beam. The beams were coupled at the ends with three degrees of freedom and the connections were theoretical point connections. The division of the rotor into beams was performed in those places where the rotor was connected to the base plate or where the cross-sectional area of the rotor altered. The dimensions of the circular beams are given in the Appendix. It was also necessary to specify for each beam its density, shear coefficient, second moment of area, damping, Young's modulus and shear modulus. This data is also given in the Appendix. The shear coefficient is a measure of how much the beam can sustain shear. It is a function of the cross-sectional shape of the beam and Poisson's ratio of the material. The damping was assumed to be hysteretic evenly distributed throughout the beam. This suffers from the same problem as the software for the experimental calculations where once a viscous damping coefficient has been calculated it is used throughout the system; however, it is possible to enter a different value of the hysteretic damping for each

substructure. It does not make a significant difference whether viscous or hysteretic damping is used. In practice a value of damping loss factor equal to 0.01 was taken as a constant for all subsystems, both rotor and plate. It is possible by further subdivision of the beam into smaller units to give damping variation similar to finite element analysis.

By applying forces to the rotor or to the base plate it was possible to predict the response at other points. By performing a logarithmic frequency sweep from 50Hz to 500Hz with 101 frequencies, inertance plots were produced. The rotor was also forced horizontally to see the effect of the base plate on the horizontal flexural modes of the rotor.

3.3 Results of Theoretical Calculations on the Rotor Test Rig

The first resonant frequency was seen at 70.6Hz. Since it was only possible to obtain modal data for the model at the ends of beams or at the nodal points of the finite element model, mode shapes could not be obtained in the same way as on the Genrad. However, by comparing the amplitude and the phase angle at various points on the plate for each resonant frequency the mode shapes were determined. The first resonance was found to be the first (3,1) doubly symmetric bending mode. An analysis of the rotor on its own shows that the first bending mode is at 78Hz. The natural frequency for the plate bending mode on its own is 77.4Hz. Hence the two components separately have a natural frequency at similar values and this results in the coupled 70.6Hz mode being quite strong. The next mode at 162Hz was the (2,2) doubly antisymmetric bending mode which was seen on the plate but not on the rotor. For the same reasons as mentioned for the experimental measurements antisymmetric plate modes do not appear on the rotor. The next mode at 177.4Hz was the (4,1) antisymmetric-symmetric plate mode which was also seen on the rotor. The next two modes were seen close together at 262Hz and 278Hz. The 262Hz mode was the (5,1) doubly symmetric plate mode, which was seen on both the plate and the rotor; the 278Hz mode was the (3,2) symmetric-antisymmetric mode which was seen on the plate only.

Some sample plots of inertance are plotted in Figure 10 showing the modes seen at different points on the plate and rotor. Having obtained inertance curves for any point on the system it is in theory straightforward to obtain the transfer function for other points merely by altering the response and force coordinates.

It has been found that the stiffness can be reduced by modelling the rotor and plate apart and putting in supports between the rotor and the plate (see Figure 11). The results obtained with this modification are as follows. It is found that the first symmetric (3,1) mode is split similarly to the experimental results with a resonance at 51Hz and a stronger resonance at 57Hz. The next resonance is virtually unchanged at 158Hz. The next mode is at 190Hz but it is not visible at the motor end of the plate or rotor. All of these modes are seen on both the rotor and the plate. The next mode is at 203Hz, which is seen on the plate only, and the following mode is at 218Hz. This appears on both the plate and the

rotor. Some of these plots are given in Figure 12.

The horizontal flexural vibration of the rotor was studied by modelling the rotor as before and modelling the supports from the rotor to the plate. The supports were fixed to ground at the base in the horizontal direction to represent the absence of horizontal motion of the base plate. That is, the plate was modelled as capable of out-of-plane vibration but not of in-plane vibration. Examples are given of the inertance response of the horizontal rotor vibrations in Figure 13. It is seen that the main modes are at 144Hz, 208Hz and 269Hz. From the vibration levels along the rotor it appears that the 208Hz mode is mainly confined to the rotating end of the rig, whereas the other two modes occur along the length of the rotor.

4. COMPARISON OF EXPERIMENTAL AND THEORETICAL VALUES

A comparison of the resonant frequencies calculated theoretically and measured experimentally, shows that in general the theoretical values are about 10-15% higher than the experimental values for the out of plane vibration of the plate and rotor. By comparison of mode shapes it is possible to match up the peaks on the plots and determine the resonant frequencies on the experimental plots which correspond with those on the theoretical plots. A list of the first five modes is given in Table 1 for comparison of theoretical and experimental values of resonant frequencies.

The reason for the increased theoretical frequency in the second column of the Table is that the model is too stiff. The physical motor/rotor assembly is offset from the plate, but the system has been modelled by connecting the rotor and plate at three points, which results in an over large stiffness and hence the frequency of the bending modes in the direction of the long sides of the plates is too large. It is observed that the percentage increase is greater for modes in which there is more than one half wavelength along the length of the shorter sides. The increase in frequency for (2,2) is 21.8% and for (3,2) is 56%. In these modes, the mode shape is confined to the plate and the rotor falls along a nodal line. When the rotor is modelled as actually lying along this line, it acts similarly to a beam stiffened plate and the resonance frequency is greatly increased.

When the model is amended by introducing beam-like supports between the plate and rotor some of the resonant frequencies are reduced. It is seen that the frequency of the first mode has been reduced. The experimental results gave a split mode (two frequencies with similar mode shapes) at 47Hz and 66Hz with the 66Hz mode stronger. The theoretical results for the amended model give resonances at 51Hz and 57Hz with the latter stronger. So there is reasonably good agreement here. The mode at 162Hz is reduced slightly to 158Hz and is present on both rotor and plate, although it is much stronger on the plate. Since the supports have been added to the model this has added 'width' to the model allowing antisymmetric modes to appear on the rotor but at a reduced level. The two modes at 262Hz and 278Hz have been reduced to 203Hz and 218Hz - a significant reduction. Experimental values for these modes are 178Hz and 232Hz.

A comparison of the horizontal flexural modes of vibration of the rotor shows that the first four experimental modes are at 104Hz, 149Hz, 205Hz and 258Hz, and the first three modes seen on the mathematical model were at 144Hz, 208Hz and 269Hz. The first experimental mode was seen to have an associated loss factor

Mode	Type	Experimental resonant frequency	Theoretical resonant frequency	% increase on experimental	Amended theoretical model frequency	% increase on experimental
1	(3,1) doubly symmetric	66.2(46.8)	71	+7	57 (51)	-14 (+9)
2	(2,2) doubly antisymmetric	132.8	162	+22	158	+19
3	(4,1) antisymmetric-symmetric	155.6	177	+14	190	+22
4	(3,2) symmetric-antisymmetric	178.6	278	+56	203	+14
5	(5,1) doubly symmetric	231.6	262	+13	218	-6

TABLE 1. Resonant frequencies for out-of-plane vibration.

of 0.127 which is suspiciously high and is seen to appear in only one of the three inertance plots in Figure 7. Discounting this mode the other modes agree well with theoretical results - to within the bounds of experimental error.

Mode	Theoretical frequency/Hz	Experimental frequency/Hz	% Increase
1	144	149	+3.5
2	208	205	-1.5
3	269	258	-4.1

The comparison of the results so far has been confined to frequency. The other important information required is the amplitude of the resonances and this is dependent upon the damping. A constant hysteretic loss factor has been assumed in the mathematical model, and estimates have been obtained of damping experimentally although the values obtained are variable and highly suspect. However, the levels for both the out of plane vibration and the horizontal vibration agree to within about 10dB.

5. CONCLUSIONS

The rotor test rig has been analysed experimentally and some mode shapes produced. The accuracy of the method is less than might be hoped with a wide range of modal parameters being produced from one structure. The values for frequencies of modal resonances show a variability of about 3% and little reliability can be placed on the values of damping obtained. With most modal analysis techniques on all but the simplest structures it is difficult to get high accuracy or good repeatability (10) without considerable effort.

Using dynamic stiffness coupling the rotor test rig was modelled to produce similar mode shapes to the experimental values. The results for the horizontal vibration were very good, lying within the bounds of experimental error. The original model for out-of-plane vibration was too stiff; modifications resulted in some improvement though some of the resulting frequencies were still too high. The modified model gave a reasonably good result for the first mode, where the mode split in a similar manner to the experimental results.

It has been seen that this substructuring method has produced results reasonably close to experimental results. However, it was found difficult to model the complete structure exactly and various approximations were used. One approximation for out of plane vibration was much too stiff. The method may be considered a half-way stage to a finite element prediction. The model is simpler than the finite element model but it can be less accurate if it does not provide as complete a physical description of the real system. For this reason it is useful to have experimental data for comparison. (It should be noted that reliable experimental data cannot always be obtained for complex structures). However, the method does provide a physical insight into the structure and enables predictions to be made with some confidence into the results which would be obtained by modifications to the structure. It should also be noted that where the results differ from experimental results they are still of a comparable magnitude - they are in the right area - and they provide an understanding of the system in that the mode shapes are comparable.

Hence, the method provides a valuable tool for the modal analysis of large machinery complexes, and for understanding their noise and vibration characteristics; also modifications to models can easily be made for the assessment of noise reduction measures.

6. ACKNOWLEDGEMENT

The experimental measurements carried out on the base plate of the rotor test rig were made by Mrs A J Buckley. Advice on the preparation of numerical data was given by Mr J H James.

D A Cordner (SO)

ARE/RJE

REFERENCES

1. DATM User Manual, Structural Dynamics Research Corporation, 1981

2. SDRC MODAL User Manual, Structural Dynamics Research Corporation, 1982

3. SCHROEDER, M R, The Statistical Parameters of the Frequency Response curves of Large Rooms, Acustica 4, Beiheft 2, p 594, 1954

4. MAIDANIK, G, Energy Dissipation Associated with Gas-pumping in Structural Joints, JASA Vol 40, 1064, 1966.

5. SAINSBURY, M G, User's Guide for the Structural Dynamic Analysis Computer Program COUPLE 1, Imperial College of Science & Technology Mechanical Engineering Department, 1975.

6. HENSHALL, R D, BENNETT, P J, McCALLION, H, and MILNER, M, Natural Frequencies and Mode Shapes of Vibration of Transformer Cores, Proc. IEE, Vol 112, No 11 pp 2133-2139, 1965.

7. HENSHALL, R D, and WARBURTON, G B. Transmission of Vibration in Beam Systems, Intl. Jnl. of Numerical Methods in Engineering Vol 1, pp 47-66, 1969.

8. ZIENKIEWICZ, O C, The Finite Element Method, 3rd Ed, McGraw Hill, 1977.

9. BLEVINS, R, Formulas for Natural Frequency and Mode Shapes, Van Nostrand, 1979.

10. EWINS, D J, A State-of-the-Art Assessment of Mobility Measurement Techniques, Imperial College of Science and Technology, Mechanical Engineering Department, 1980.

APPENDIX

BEAM DATA FOR ROTOR

The material properties of steel were used: Density 7850 kgm^{-3}
Young's modulus $0.207 \times 10^{12} Nm^{-2}$
Shear modulus $0.796 \times 10^{11} Nm^{-2}$

The Timoshenko shear coefficient is 0.886 for circular beams in which Poisson's ratio is 0.3.

Additionally the following data were specified for each beam: length, cross-sectional area, second moment of area in bending, polar moment of area, and torsional constant. For circular beams the torsional constant is equal to the polar moment of area, and the polar moment of area is twice the second moment of area in bending.

	Length (m)	Cross-sectional area (m^2)	Second moment of area (m^4)
Beam 1 Motor Back End	0.125	3.142×10^{-2}	7.854×10^{-5}
Beam 2 Motor Front End	0.125	3.142×10^{-2}	7.854×10^{-5}
Rod 1	0.04	3.142×10^{-4}	7.854×10^{-9}
Rod 2	0.09	3.848×10^{-3}	1.179×10^{-6}
Rod 3	0.25	3.142×10^{-4}	7.854×10^{-9}
Rod 4	0.32	2.827×10^{-3}	6.362×10^{-7}
Cylinder	0.30	2.545×10^{-2}	5.153×10^{-5}
Rod 5	0.06	1.257×10^{-3}	1.257×10^{-7}

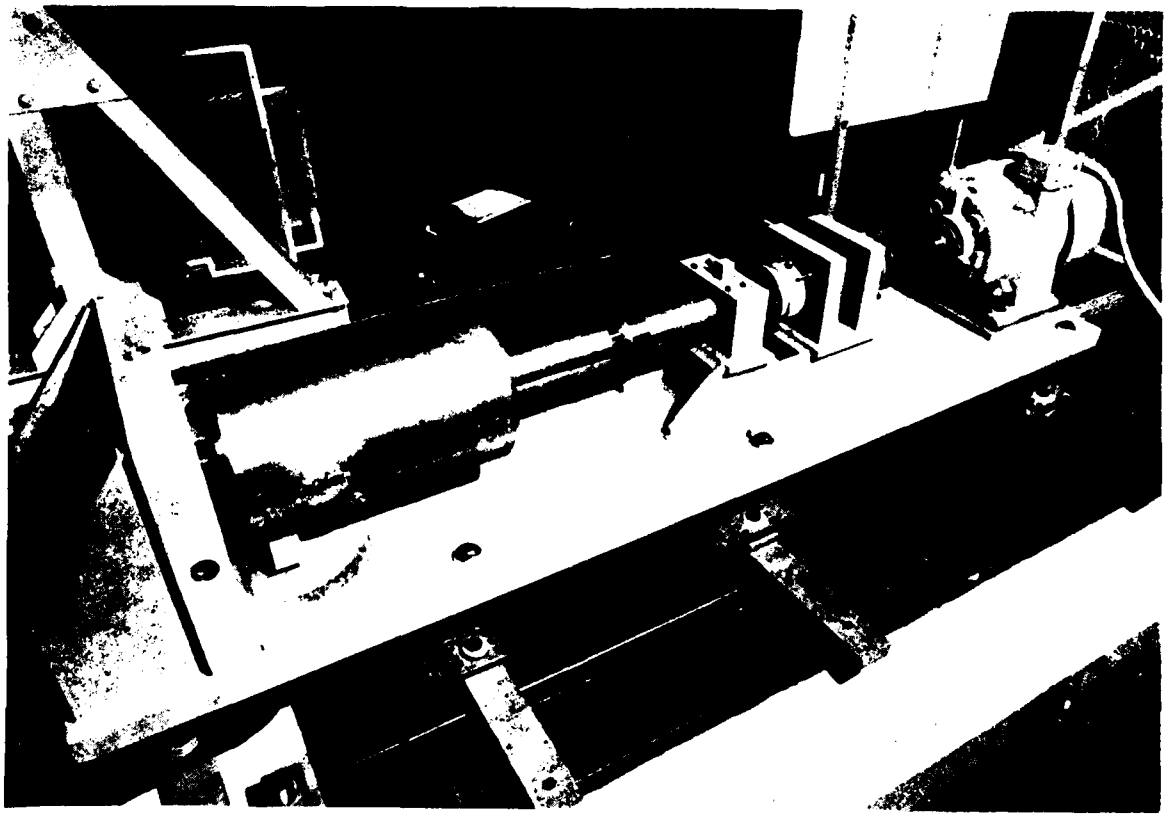

FIG. 1(a) THE ROTOR TEST RIG

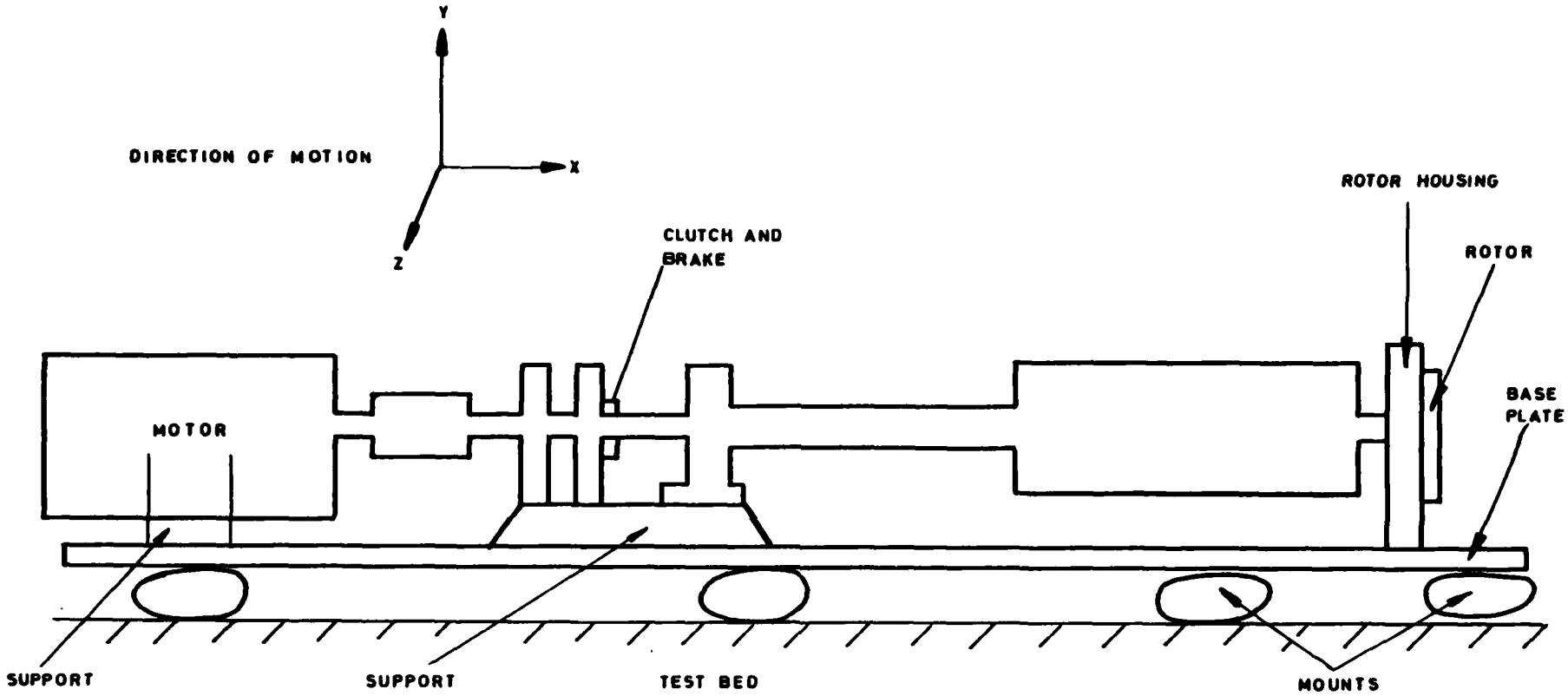

FIG. 1(b) DIAGRAM OF THE ROTOR TEST RIG

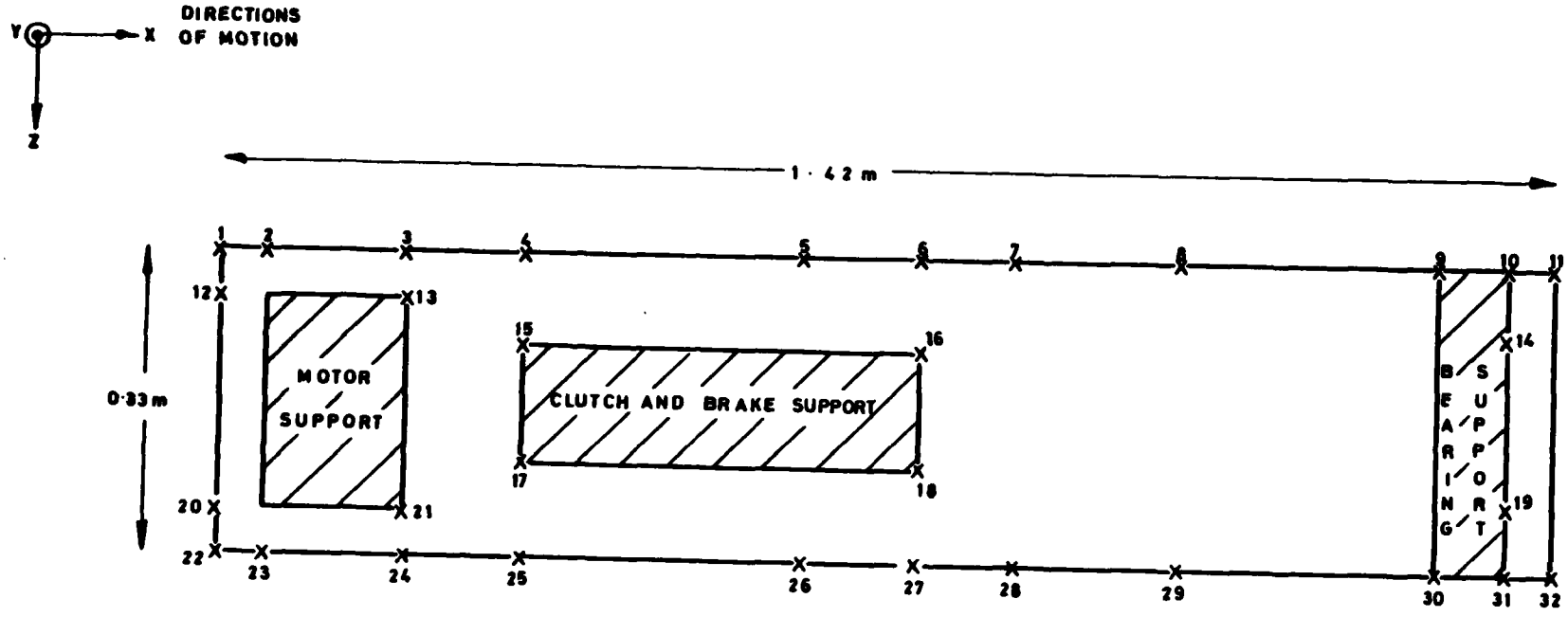

FIG. 2 PLAN VIEW OF MEASUREMENT LOCATIONS ON BASE PLATE

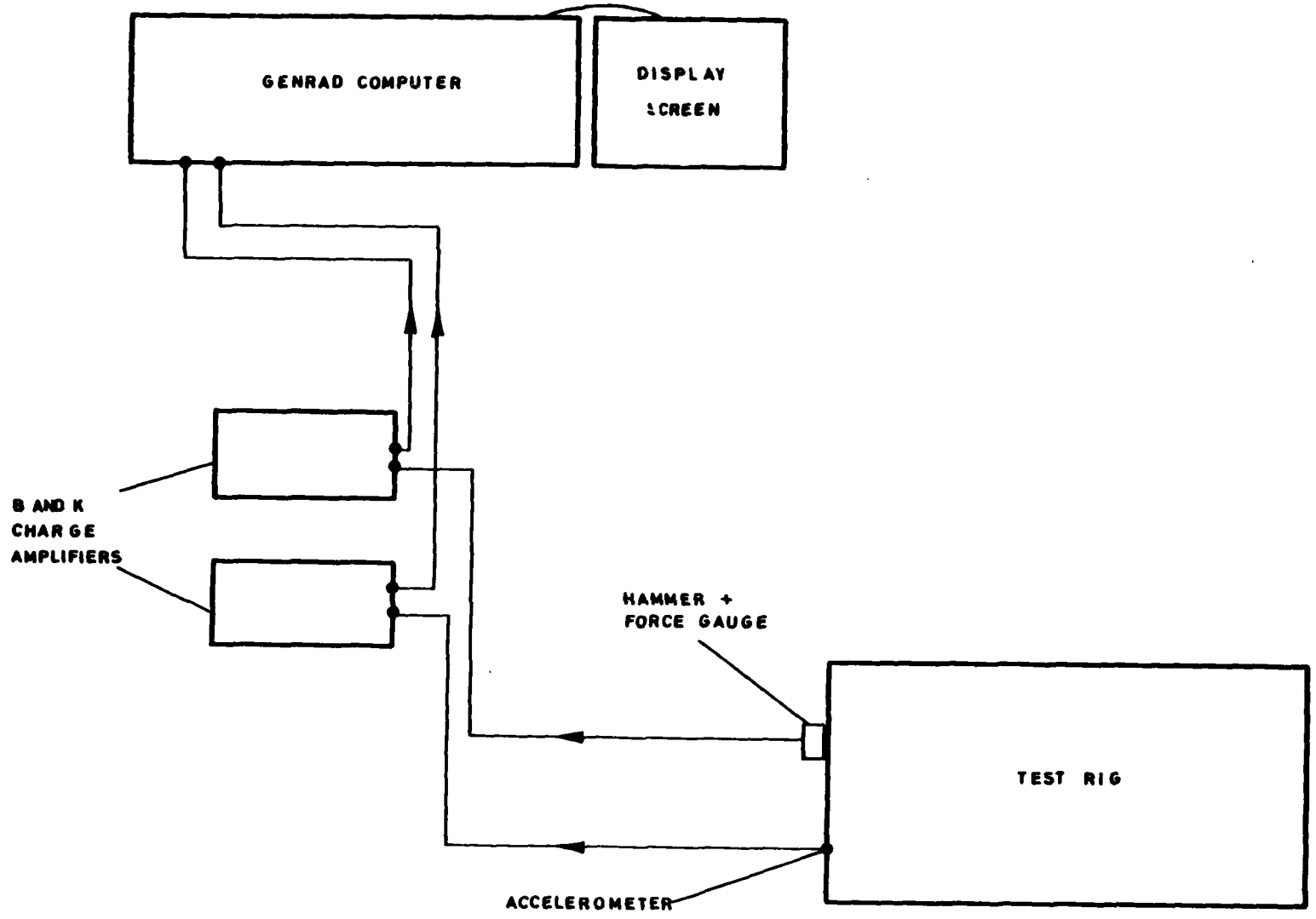

FIG.3 LINE DIAGRAM OF THE INSTRUMENTATION

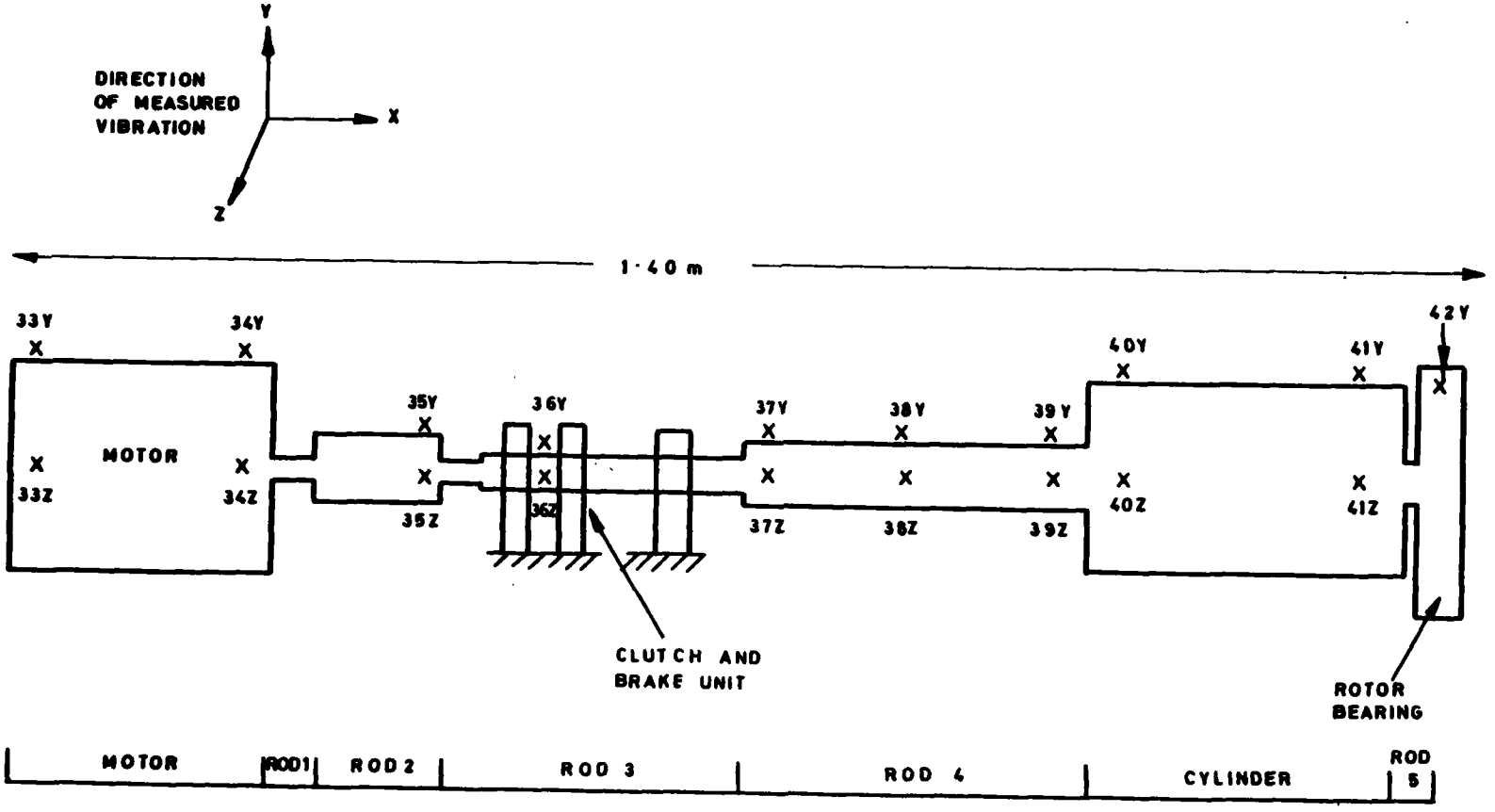

FIG. 4 SIDE VIEW OF ROTOR WITH MEASUREMENT LOCATIONS

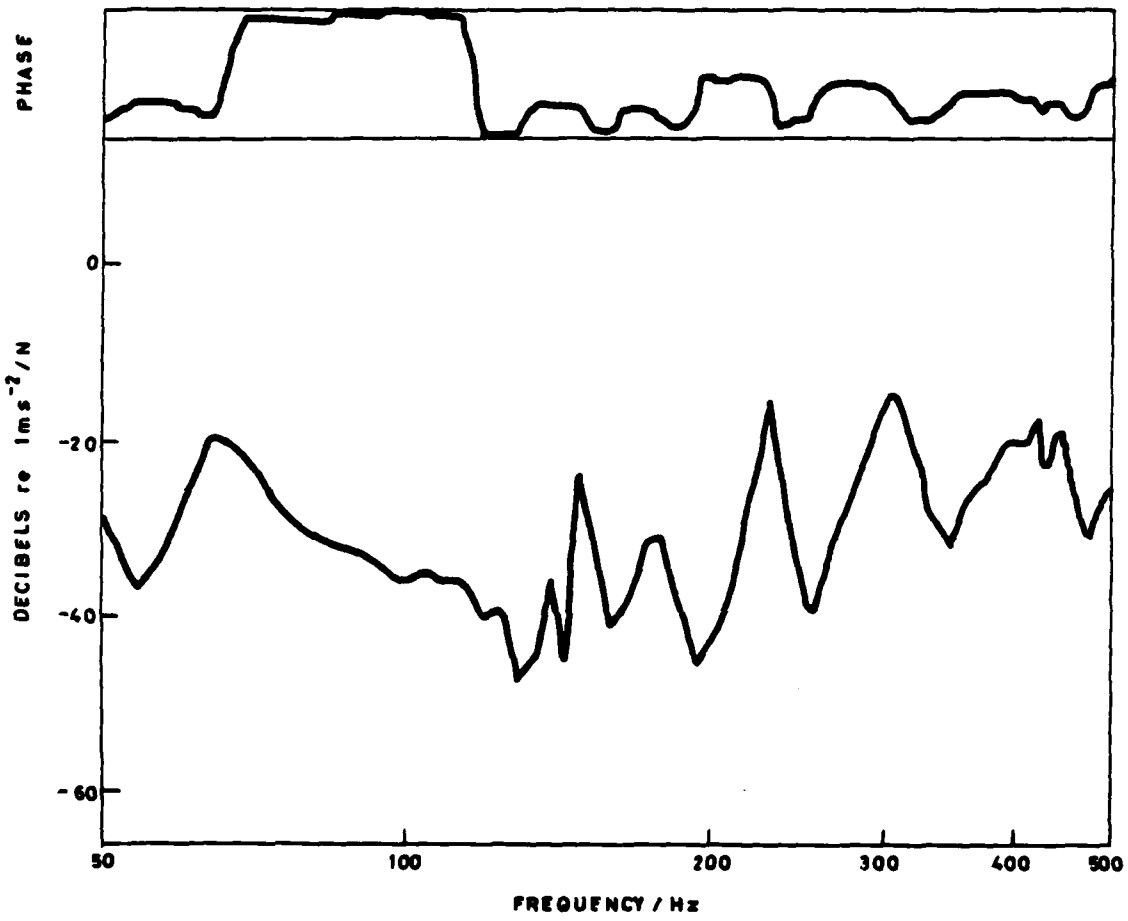

FIG. 5 (a) DRIVING POINT INERTANCE ON ROTOR

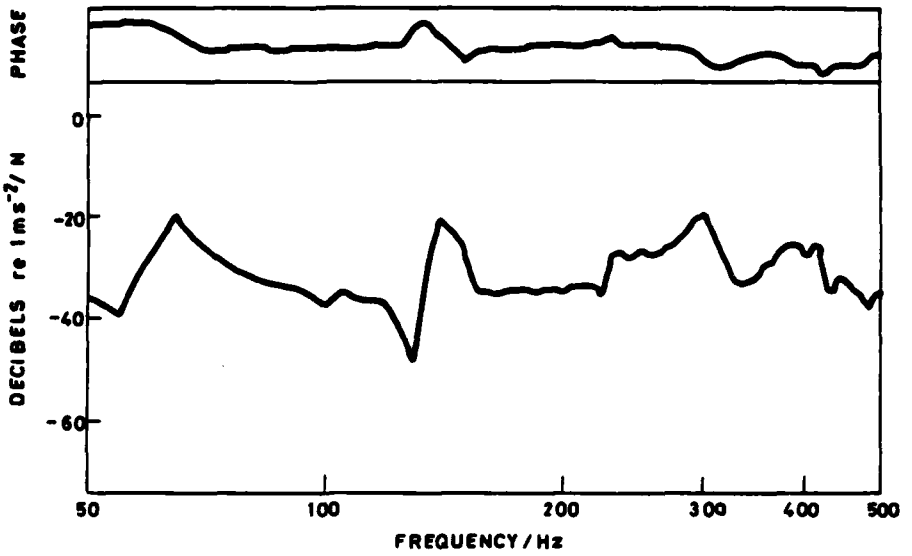

FIG. 5(b) INERTANCE AT POSITION 2

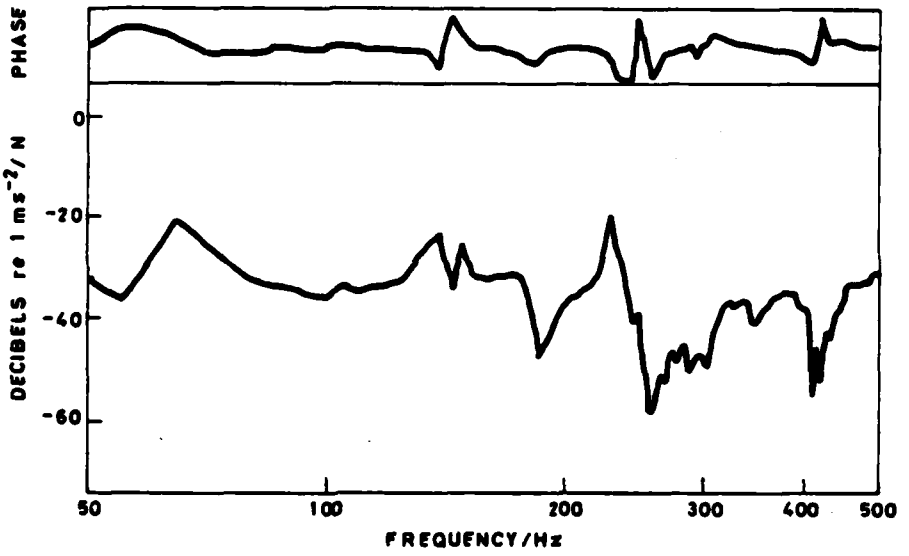

FIG. 5(c) INERTANCE AT POSITION 10

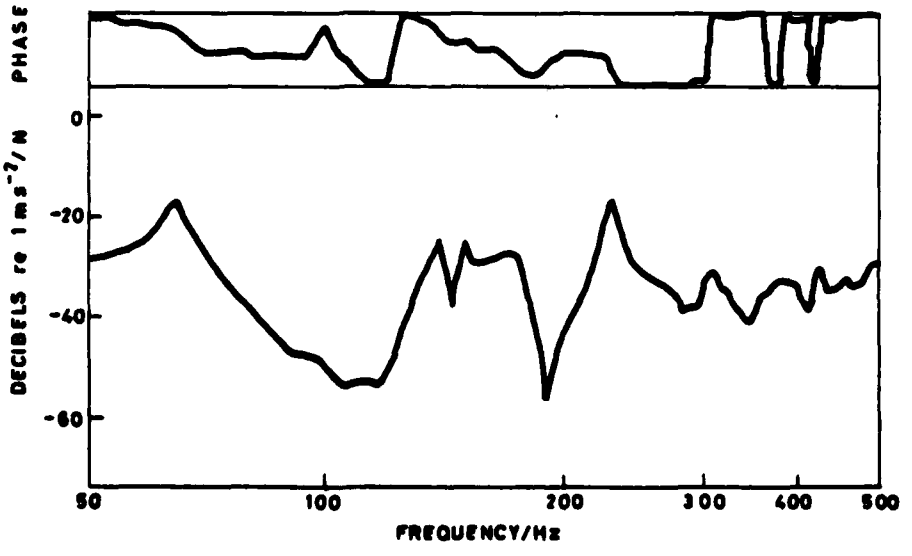

FIG. 5(d) INERTANCE AT POSITION 32

motor end

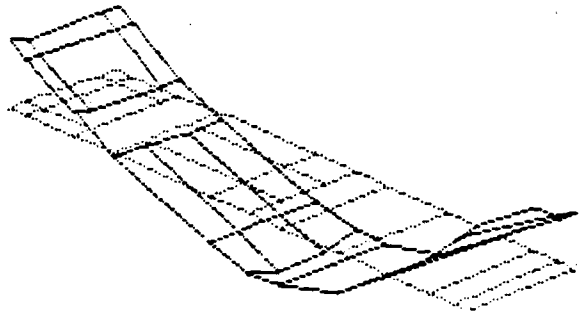

FIG 6(a) FIRST BENDING MODE ON PLATE 66Hz

motor end

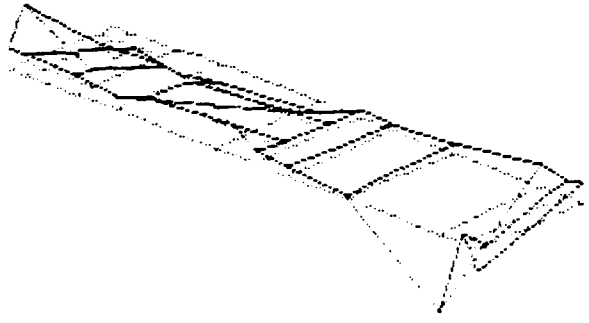

FIG 6(b) FIRST DOUBLY ANTISYMMETRIC PLATE MODE 133Hz

motor end

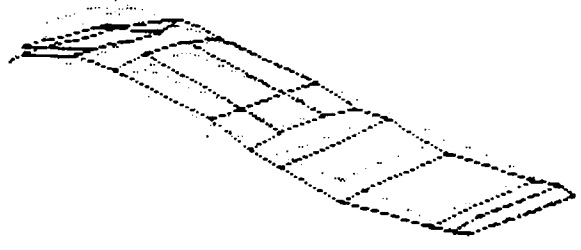

FIG 6(c) ANTISYMMETRIC-SYMMETRIC PLATE MODE 156Hz

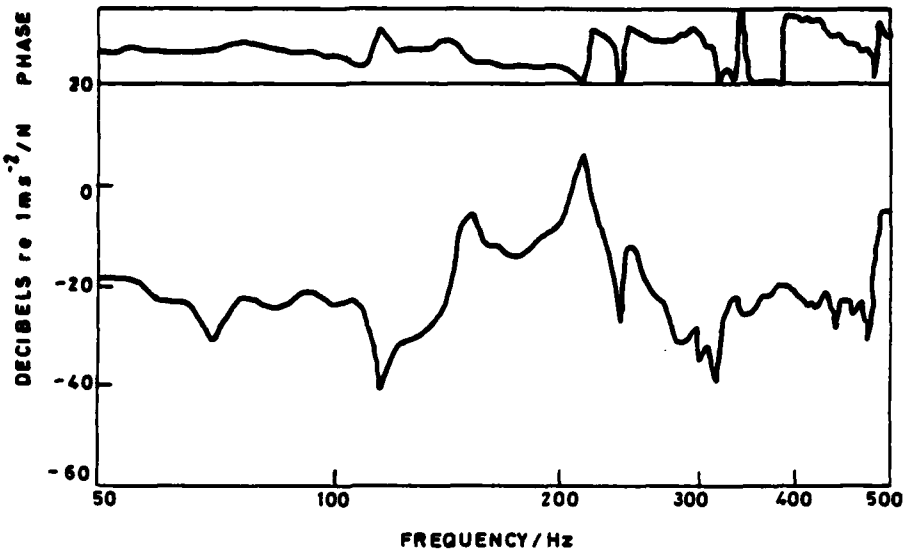

FIG. 7(a) HORIZONTAL VIBRATION OF ROTOR POSITION 33Z-

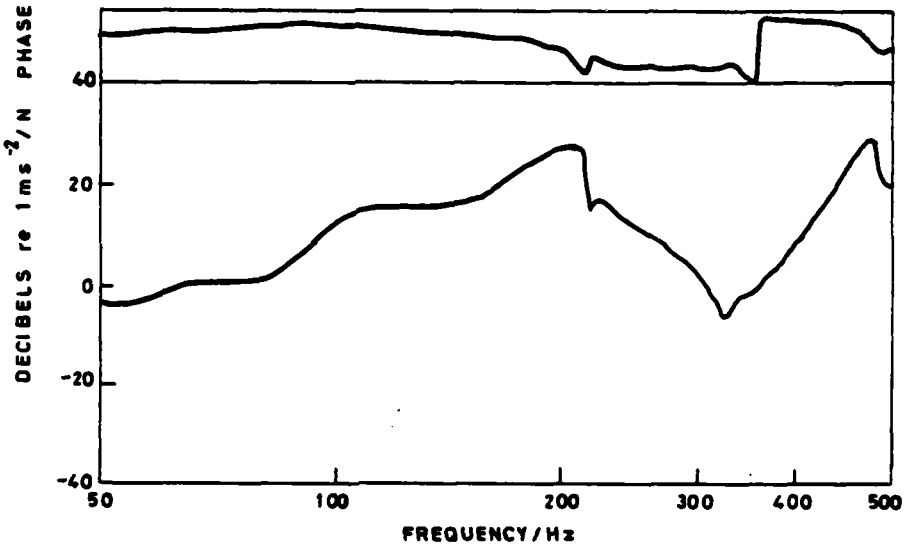

FIG. 7(b) HORIZONTAL VIBRATION OF ROTOR, DRIVING POINT 39Z-

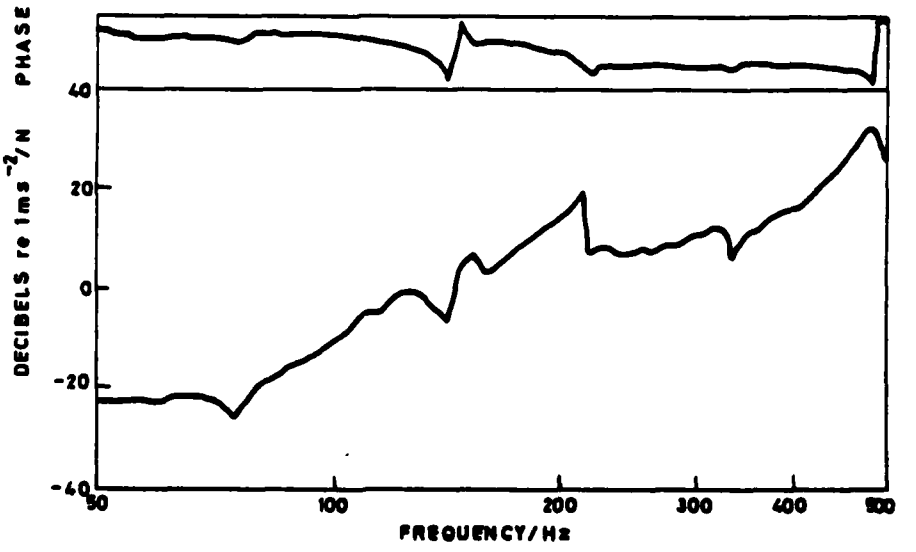

FIG. 7(c) HORIZONTAL VIBRATION OF ROTOR POSITION 41Z-

NUMBERS REFER TO POSITIONS MARKED IN FIG. 4

FIG. 8 (a) 1st HORIZONTAL MODE 104Hz VIEW FROM TOP

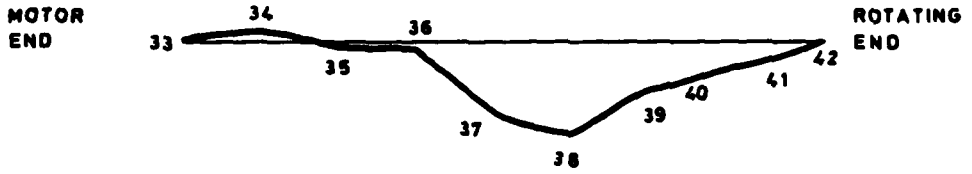

FIG. 8(b) 2nd HORIZONTAL MODE 149Hz VIEW FROM TOP

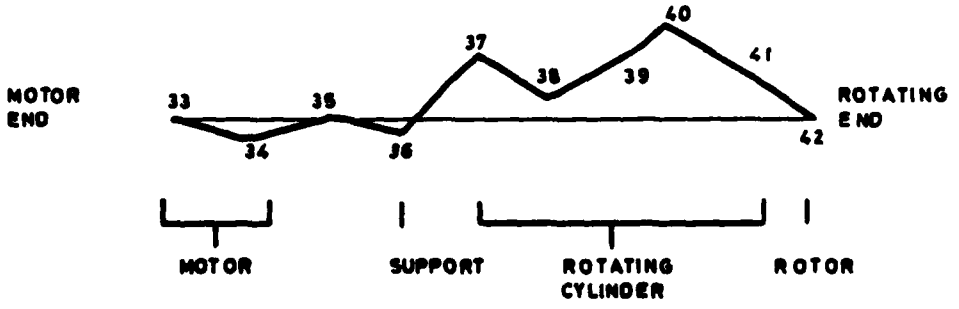

FIG. 8 (c) 3rd HORIZONTAL MODE 205Hz VIEW FROM TOP

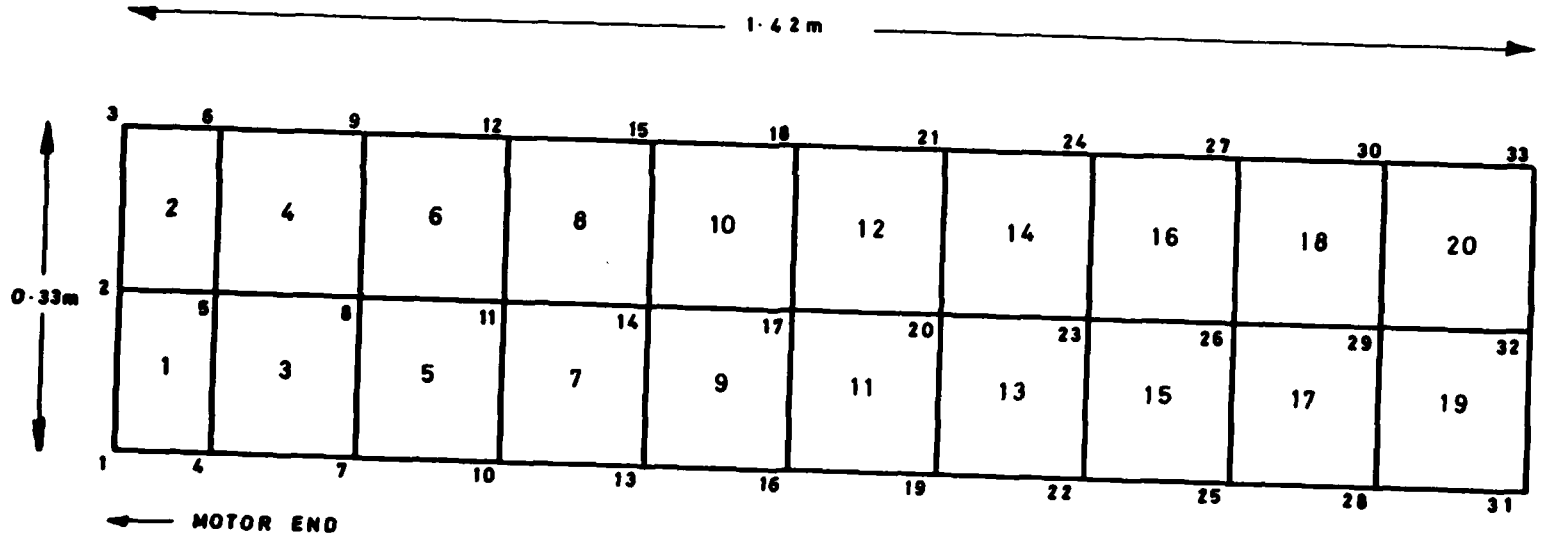

FIG. 9 DIVISION OF PLATE INTO ELEMENTS WITH ELEMENT NUMBERS AND NODE NUMBERS

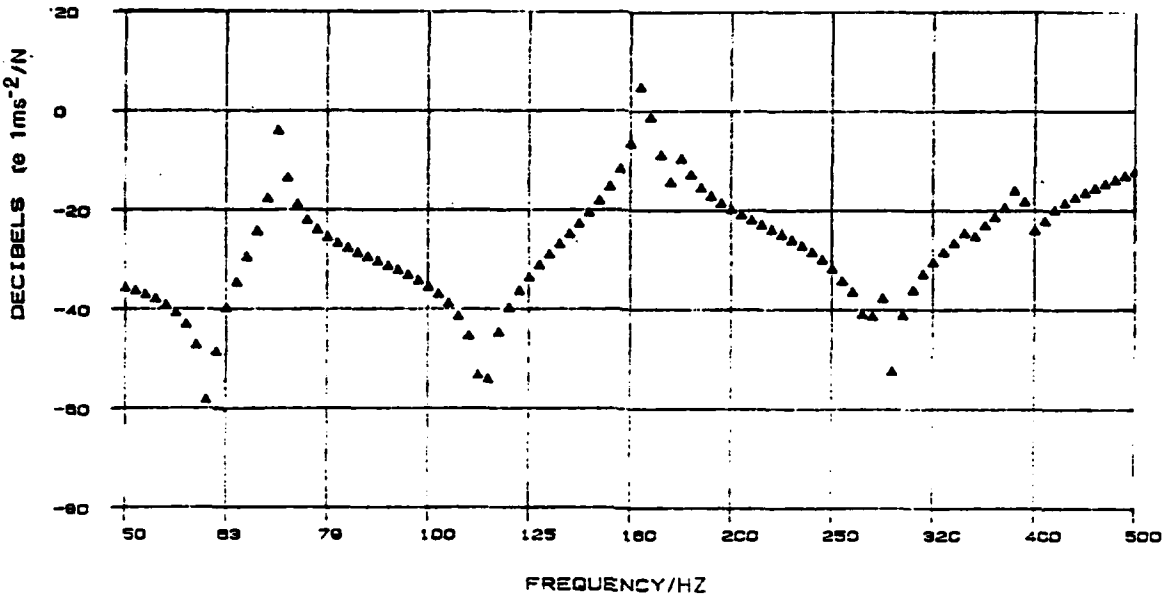

FIG 10(a) DRIVING POINT INERTANCE AT NODE 3 ON PLATE

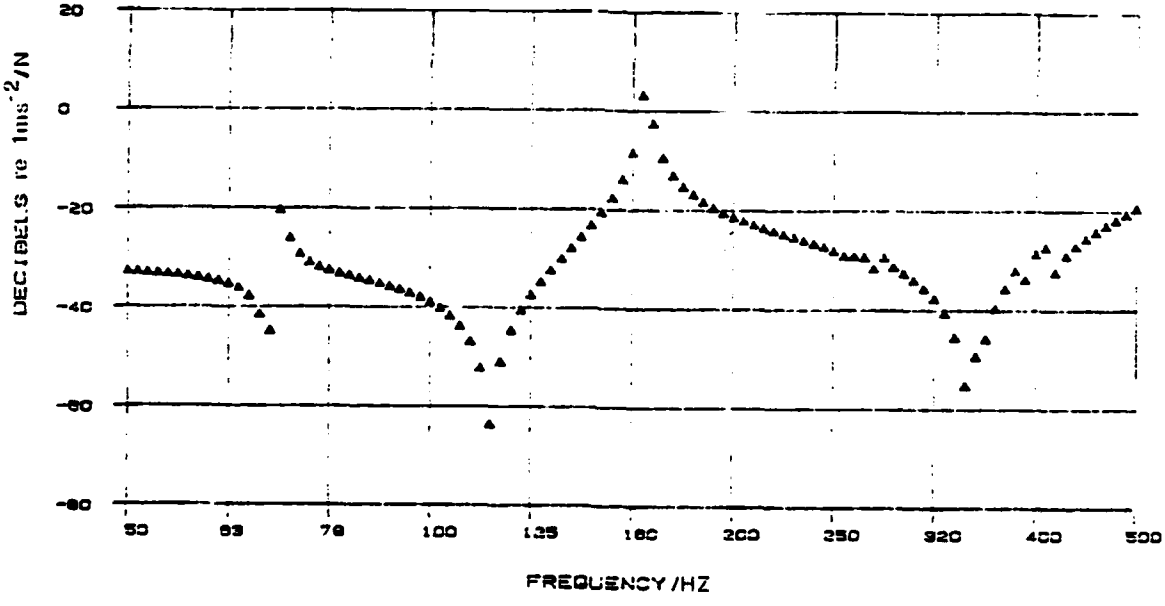

FIG 10(b) DRIVING POINT INERTANCE AT NODE 6 ON PLATE

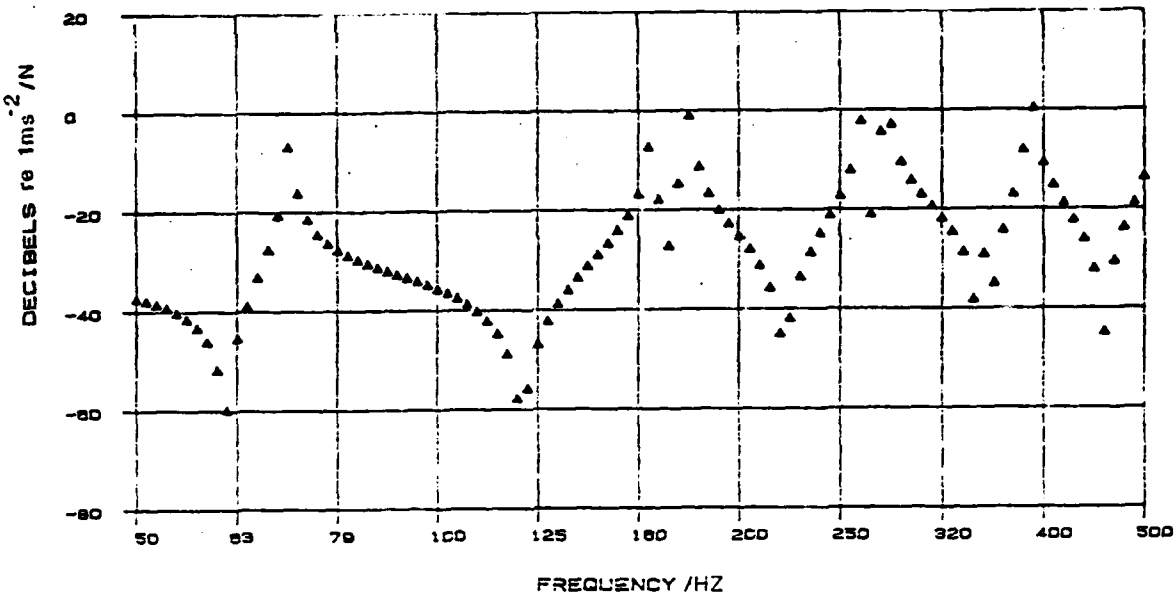

FIG 10(c) DRIVING POINT INERTANCE AT NODE 21 ON PLATE

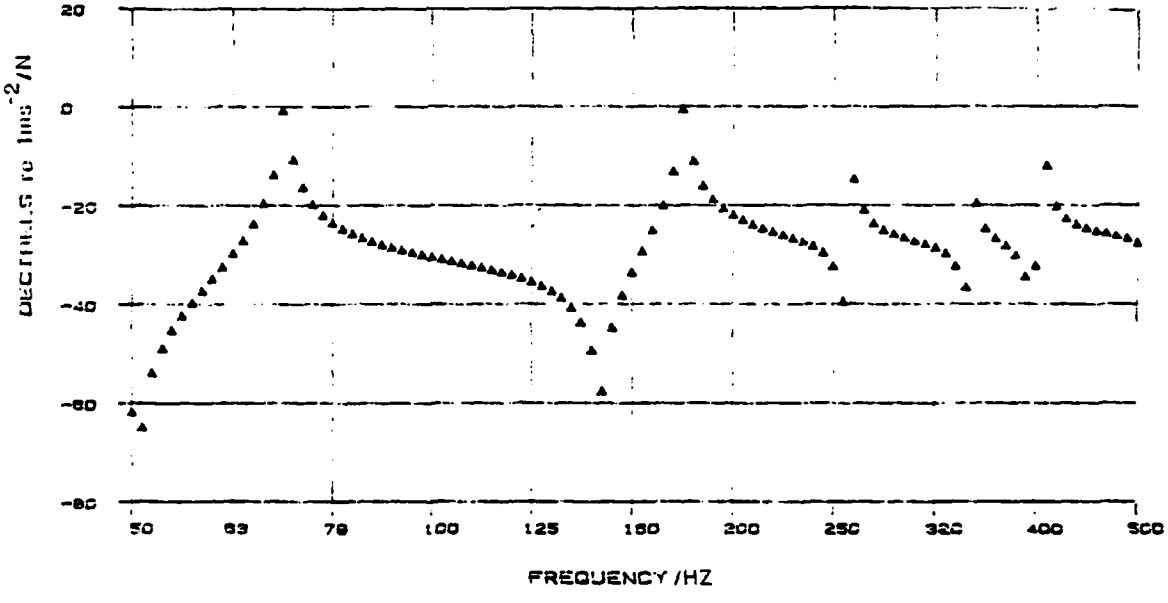

FIG 10(d) DRIVING POINT INERTANCE AT BACK END OF MOTOR

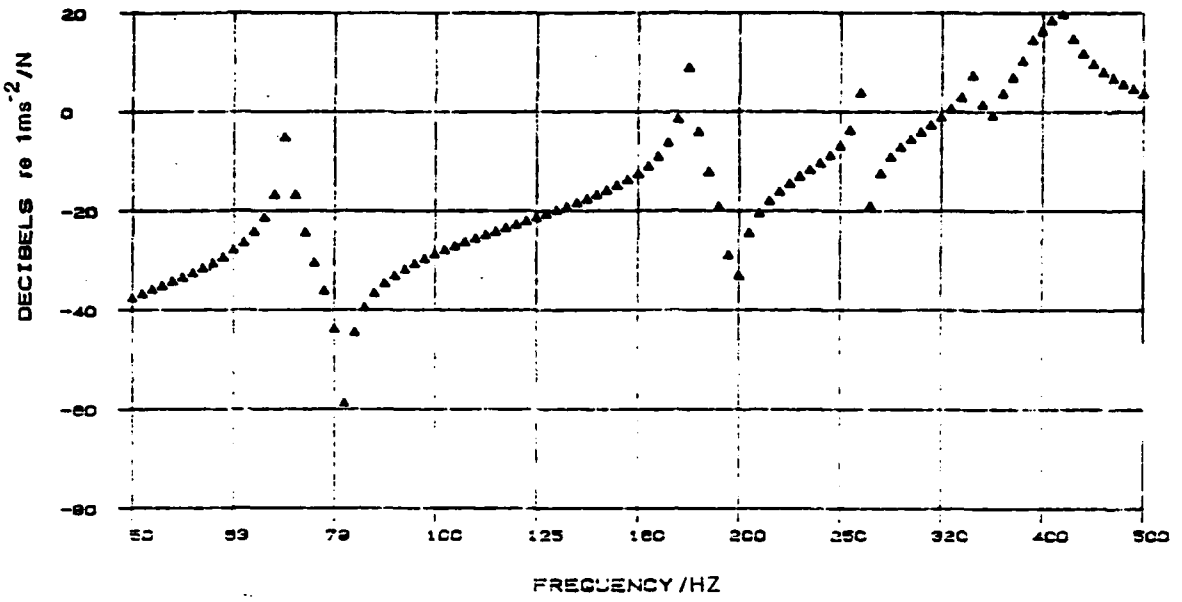

FIG 10(e) DRIVING POINT INERTANCE BY CLUTCH AND BRAKE SUPPORT

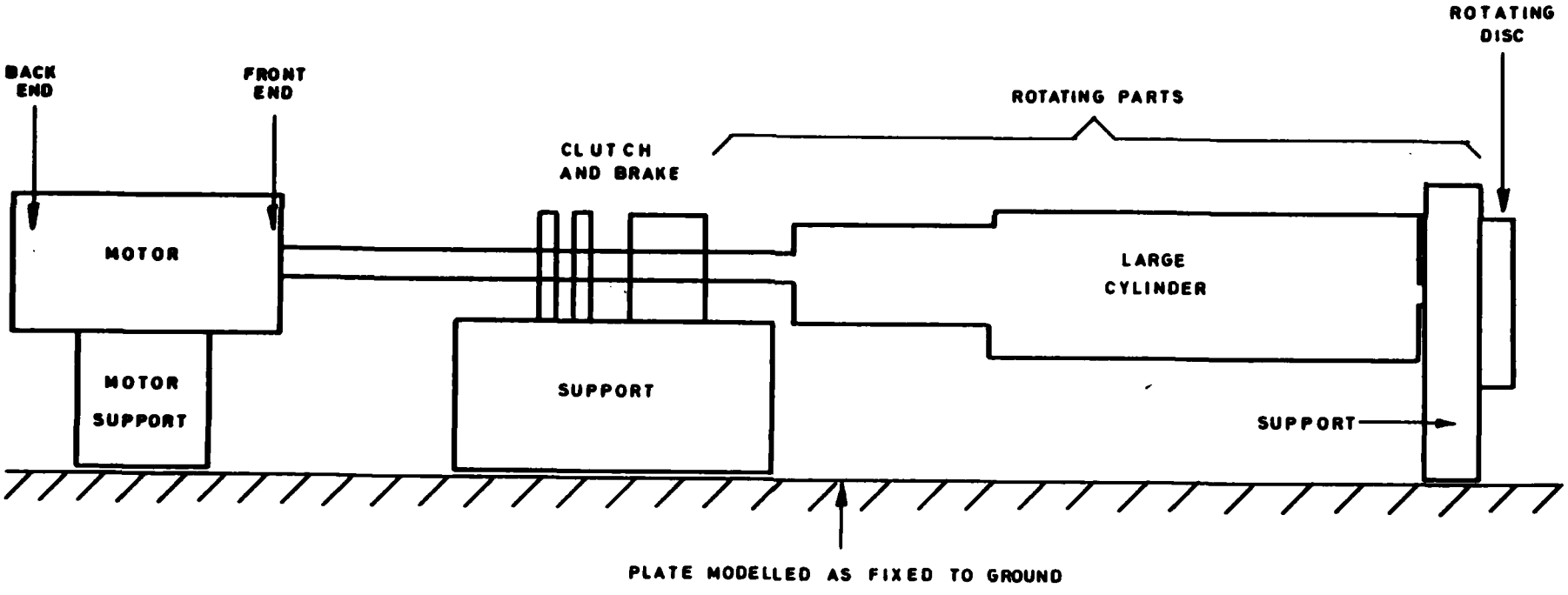

FIG. 11 MODEL FOR VIBRATION OF ROTOR WITH SUPPORTS

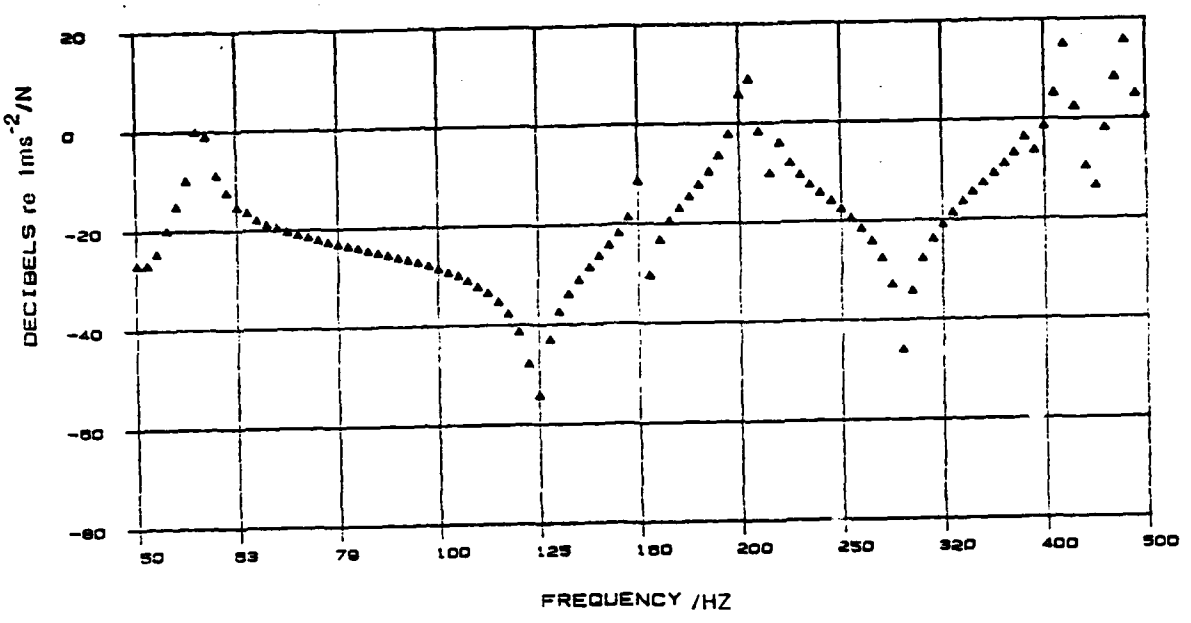

FIG 12(a) DRIVING POINT INERTANCE AT NODE 1 ON PLATE

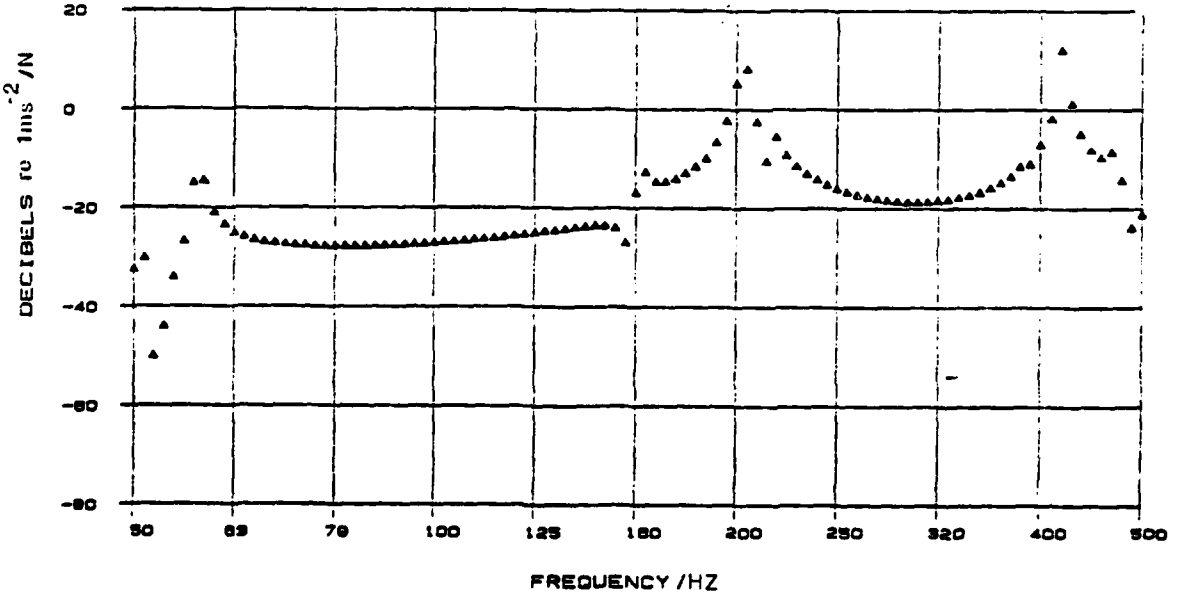

FIG 12(b) TRANSFER INERTANCE AT NODE 28 ON PLATE

FORCING AT NODE 1

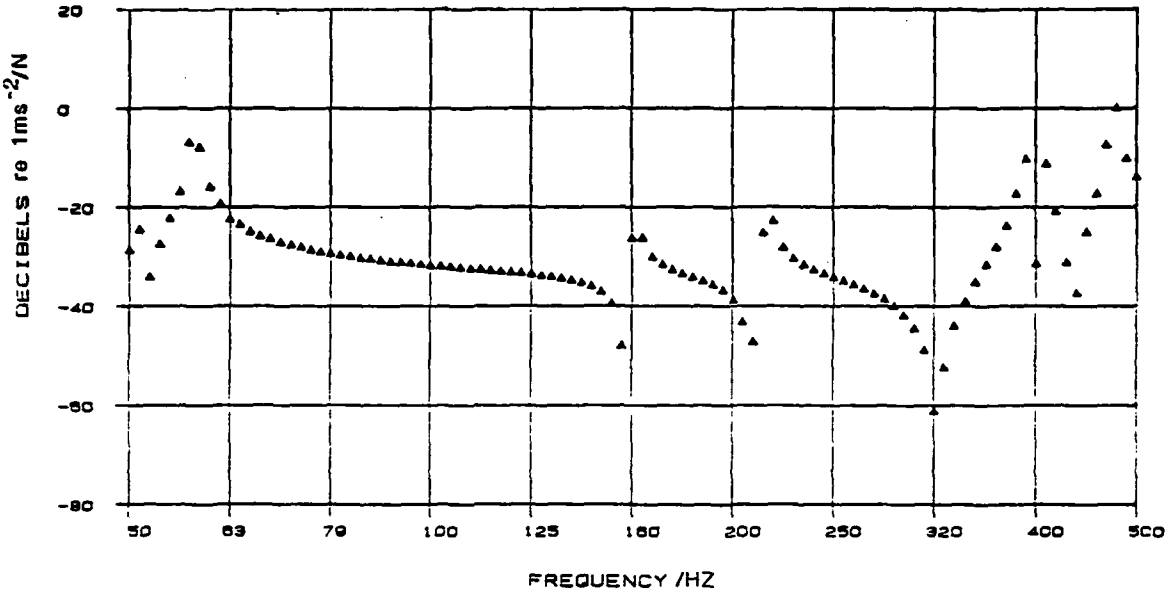

FIG 12(c) DRIVING POINT INERTANCE AT BACK END OF MOTOR

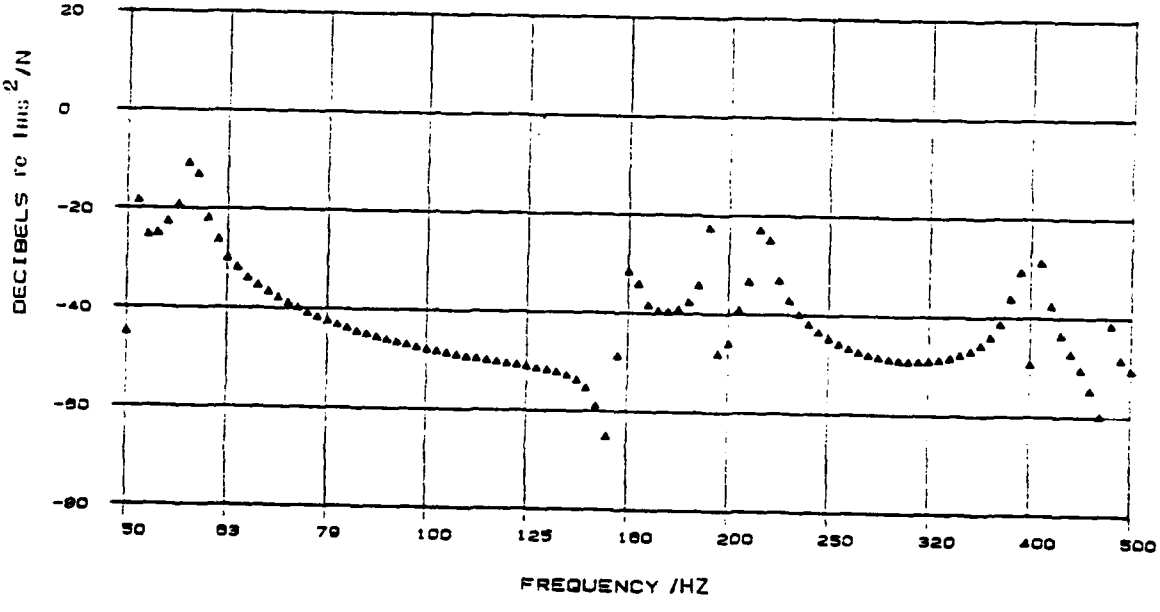

FIG 12(d) TRANSFER INERTANCE AT FAR END OF ROTOR

FORCING AT BACK END OF MOTOR

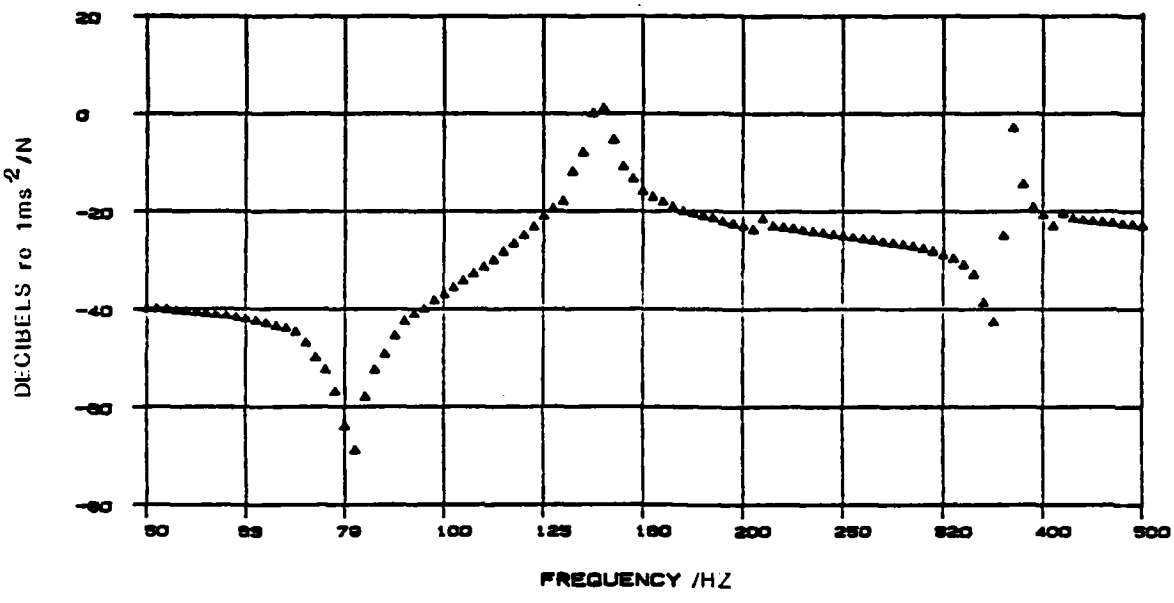

FIG 13(a) DRIVING POINT INERTANCE
HORIZONTAL FLEXURAL VIBRATION AT BACK END OF MOTOR

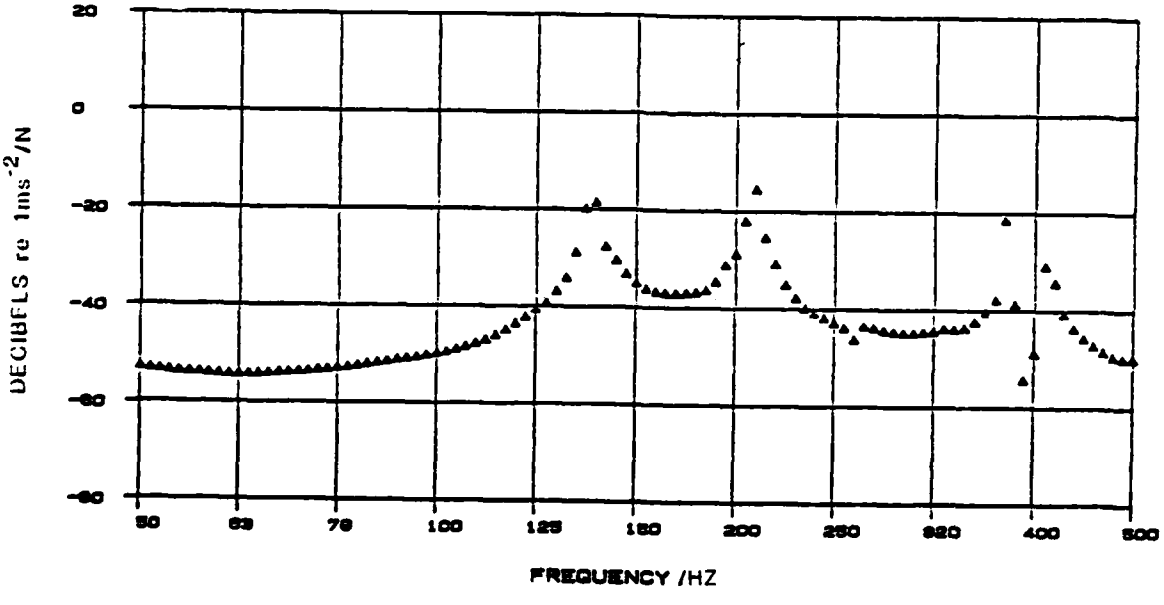

FIG 13(b) HORIZONTAL FLEXURE AT FAR END OF ROTOR
FORCING AT BACK END OF MOTOR